PATH OPTIMIZATION FOR AN EARTH-BASED DEMONSTRATION BALLOON FLIGHT

DANIEL BEYLKIN

Mentor: Jerrold Marsden
Co-Mentors: Claire Newman, Philip Du Toit, and Marin Kobilarov

ABSTRACT. In this paper, we present an approach to autonomous navigation of a balloon by optimally exploiting wind fields to minimize control (i.e. power requirements), time of travel, or other cost functionals. We use the principles of Discrete Mechanics and Optimal Control (DMOC) to compute optimal trajectories for a simplified model of balloon dynamics in a two-dimensional, time-dependent wind velocity field. The wind field was produced using the Weather Research and Forecasting (WRF) model for a region of the Mojave Desert on July 5, 2005.

Due to inherent inaccuracies of the global wind model and the need for efficient optimization, we approach the problem of optimizing medium-scale (i.e., distances of the order approximately 100km) balloon trajectories using a simplified model of balloon dynamics. The results presented in this paper provide a framework to extend this approach to finding optimal trajectories in real-time for a three-dimensional wind field.

We hope to test our approach during a balloon demonstration flight currently planned to take place in the Mojave Desert in 2009. Results of such experiment may be used to develop an approach for a similar problem of autonomous and optimal balloon navigation on Titan, a moon of Saturn.

1. INTRODUCTION

The Cassini-Huygens spacecraft mission to study Saturn revealed remarkable observations of Titan, Saturn's moon. The data sent back to Earth demonstrates the likely existence of high-latitude hydrocarbon oceans [3] and equatorial sand dunes [5]. The rocks on the surface are likely made up of water-ice pebbles, analogous to the silicate sands found on Earth [4]. While life is unlikely to exist on Titan, its uncanny similarities to Earth have sparked the interest and curiosity of the scientific community.

An overview of some of the most intriguing scientific questions can be found in [12, 13]. These include, but are not limited to, a study of the geochemical processes on Titan and their similarities to those found on Earth, a study of the prebiotic chemistry on Titan, and a study into the origin and evolution of Titan. Answering these questions would require greater surface exploration than is currently possible with the Cassini-Huygens mission. If NASA were to return to Titan, aerobots and Montgolfier balloons have been proposed for scientific exploration of Titan's surface [2]. Ideally the vehicle would be able to gather data for an extended period of time, hopefully greater than six months, while circumnavigating Titan with the possibility of conducting some surface sampling experiments.

While the balloon is on Titan, intervening with the flight-plan on a short time-scale is impossible. In addition to a communication lag time of several hours, there will be communication blackout periods where the balloon will be operating in largely unknown environments [2]. Therefore, it is necessary for the balloon to make decisions autonomously and still be able to reach particular regions of interest on Titan in order to gather high quality data. It is hoped that by optimally exploiting the winds on Titan, the balloon would be able to autonomously navigate different regions of Saturn's moon with minimal control force or time of travel.

It is not exactly clear what type of information the balloon will have regarding the wind fields. Several global wind models for the atmosphere of Titan exists although they are not very robust. Moreover, they can help the balloon navigate Titan globally, but locally may not be of much use. We note that even with perfect information this problem is not easy to solve.

The launch of a Titan-exploration mission will occur no earlier than 2016 [13]. Until then, some experiments will be run on Earth to test methods that can be used to solve the problem on Titan. If an approach is to succeed on Titan, it should also work on Earth, whose atmospheric models are much more robust and reliable due to a greater availability of accurate data and verifiable results. For Earth, we use a mesoscale weather model that can provide us with wind data for a relatively small area with higher resolution than would be available with a global model.

The problem of optimal balloon navigation in the presence of winds is not limited to a Titan mission. Such aerial vehicles may be useful for further study of atmospheric phenomena on Earth or may be used for surveillance, exploration, or even transportation of goods.

We are primarily concerned with medium-scale (i.e., distances of 100km) balloon navigation for which the global wind model should help us compute a near-optimal trajectory. Then, in order to traverse this trajectory, the balloon would use local wind information (it gathers) to maneuver on scales of 10-100m. However, such small-scale balloon navigation is a somewhat different problem than the medium-scale problem with which we are concerned.

2. Discrete Mechanics and Optimal Control

2.1. **Framework.** We are concerned with an optimal control problem for a balloon in a wind field. We employ the DMOC framework [9, 11] for this problem. Abstractly, we want to compute the control, $\mathbf{f}(t)$, necessary to move a balloon in configuration space Q from an initial state $(\mathbf{q}_{ini}, \dot{\mathbf{q}}_{ini})$ to a final state $(\mathbf{q}_{fin}, \dot{\mathbf{q}}_{fin})$, while minimizing the cost functional

$$(2.1) \qquad J(\mathbf{q}, \mathbf{f}) = \int_0^T C(\mathbf{q}(t), \dot{\mathbf{q}}(t), \mathbf{f}(t))dt.$$

However, we must constrain $\mathbf{q}(t)$ so that the balloon obeys physical laws. Usually DMOC requires the motion must satisfy the Lagrange-d'Alembert principle, but we will constrain $\mathbf{q}(t)$ using the equations of motion derived from Newton's second law instead. In some cases, an appropriate descretization (i.e., Midpoint Rule) of the associated ordinary differential equations will perform as well as the variational approach. We choose to approximate the balloon as a fixed-size sphere since more complex motion constraints will significantly slow down the computation, but will

not significantly influence the trajectory for the medium-scale problem. On the other hand, solving small-scale problems may require greater sophistication.

2.2. **Newton's Laws.** In three dimensions, the principle forces acting on the balloon are lift, gravity, drag, and propulsion. In the horizontal directions, there is no lift or gravity, so propulsion is the only controlling force. In the vertical direction, we combine the lift, gravity, and propulsion. However, we first considered a two dimensional model which neglects the altitude. Implementing the model in three dimensions is part of the future research goals - see Section (4.1).

We define the following variables:

- ρ: density. We will say that ρ_{fluid} refers to the air and ρ_{gas} refers to the gas inside the balloon. Note that ρ_{fluid} depends on elevation, temperature, etc, however, for simplicity, we will assume this is constant. In hot air balloons, ρ_{gas} is controlled by changing its temperature. Again, for now, we will assume that ρ_{gas} is constant.
- V: volume, specifically of the balloon. We may assume the balloon is a sphere, in which case the cross-sectional area $A = \pi R^2$ and $V = \frac{4}{3}\pi R^3$. Depending on the design, the volume of the balloon could depend on elevation, temperature, etc, however again, we assume this is constant.
- m_{eq}: mass of the equipment.
- D: drag coefficient .
- $\mathbf{v}$ refers to velocity of the wind. We definite the scalar quantity

$$\|\mathbf{v} - \dot{\mathbf{x}}\| = \sqrt{(v_x - \dot{x})^2 + (v_y - \dot{y})^2}$$

  where v_x, v_y are the components of the wind velocity and $\dot{x}, \dot{y}$ are the components of the balloon velocity in the $e_x = (1, 0, 0)$, $e_y = (0, 1, 0)$ directions.

Drag due to the wind, assuming quadratic dependence on relative velocity, pushes against the direction of motion of the balloon. We have (in a vector form)

$$\mathbf{F}_d = -\frac{1}{2}\rho_{\text{fluid}}\|\mathbf{v} - \dot{\mathbf{x}}\|^2 DA\frac{\mathbf{v} - \dot{\mathbf{x}}}{\|\mathbf{v} - \dot{\mathbf{x}}\|}$$

$$= -\frac{1}{2}\rho_{\text{fluid}}\|\mathbf{v} - \dot{\mathbf{x}}\| DA(\mathbf{v} - \dot{\mathbf{x}}).$$

Overall, if we include the control force, $\mathbf{f}_c$, we have

$$(m_{\text{eq}} + \rho_{\text{gas}}V)\ddot{\mathbf{x}} = -\frac{1}{2}\rho_{\text{fluid}}\|\mathbf{v} - \dot{\mathbf{x}}\| DA(\mathbf{v} - \dot{\mathbf{x}}) + \mathbf{f}_c.$$

If we introduce the following quantities

$$\beta = \frac{\rho_{\text{fluid}}DA}{2(m_{\text{eq}} + \rho_{\text{gas}}V)}$$

and

$$\tilde{\mathbf{f}}_c = \frac{\mathbf{f}_c}{m_{\text{eq}} + \rho_{\text{gas}}V},$$

then we have

$$\ddot{\mathbf{x}} = -\beta\|\mathbf{v} - \dot{\mathbf{x}}\|(\mathbf{v} - \dot{\mathbf{x}}) + \tilde{\mathbf{f}}_c.$$

If we set $\mathbf{q} = \mathbf{x}$ and $\mathbf{p} = \dot{\mathbf{x}}$, we get

(2.2)
$$\dot{\mathbf{q}} = \mathbf{p},$$

$$\dot{\mathbf{p}} = -\beta\|\mathbf{v} - \mathbf{p}\|(\mathbf{v} - \mathbf{p}) + \tilde{\mathbf{f}}_c.$$

We set β by using an approximation to the specifications of the JPL aerobot [2].

It is clear that the wind plays an critical role in (2.2). For a more thorough discussion of the wind field and how it is generated using the Weather Research and Forecasting model, see Appendix (5.1).

2.3. **Discretization.** We approximate the balloon trajectory, $\mathbf{q} : [0, t_{final}] \to Q$ using a discrete path $\mathbf{q}_d : \{0, h, 2h, \ldots, Nh, (N+1)h = t_{final}\} \to Q$ such that $\mathbf{q}_d(kh) \approx \mathbf{q}(kh)$. We approximate $\mathbf{p}$ by $\mathbf{p}_d$ and $\tilde{\mathbf{f}}_c$ by $\mathbf{f}_d$ in an analogous manner. We impose the boundary conditions, that is $\mathbf{q}_d(0) = \mathbf{q}_{ini}$, $\mathbf{p}_d(0) = \dot{\mathbf{q}}_{ini}$, $\mathbf{q}_d(t_{final}) = \mathbf{q}_{fin}$, and $\mathbf{p}_d(t_{final}) = \dot{\mathbf{q}}_{fin}$.

2.3.1. *Discrete Newton's Law.* There are many ways to discretize (2.2). We use the Midpoint Rule which provides an appropriate balance of numerical precision (i.e., it is second-order, implicit, and symplectic) and computational efficiency. We have

$$(2.3) \qquad \mathbf{q}_{n+1} = \mathbf{q}_n + h\left(\frac{\mathbf{p}_{n+1} + \mathbf{p}_n}{2}\right),$$

$$\mathbf{p}_{n+1} = \mathbf{p}_n + h\left(-\beta\|\mathbf{v}_{\frac{2n+1}{2}} - \frac{\mathbf{p}_{n+1} + \mathbf{p}_n}{2}\|(\mathbf{v}_{\frac{2n+1}{2}} - \frac{\mathbf{p}_{n+1} + \mathbf{p}_n}{2}) + \mathbf{f}_n\right),$$

where $\mathbf{v}_{\frac{2n+1}{2}} = \mathbf{v}(\frac{\mathbf{q}_{n+1} + \mathbf{q}_n}{2})$. As described, we must impose the boundary conditions, $\mathbf{q}_0 = \mathbf{q}_{ini}$, $\mathbf{p}_0 = \dot{\mathbf{q}}_{ini}$, $\mathbf{q}_{N+1} = \mathbf{q}_{fin}$, and $\mathbf{p}_{N+1} = \dot{\mathbf{q}}_{fin}$.

2.3.2. *Discrete Cost Functional.* We approximate the cost functional (2.1) as

$$J_d(\mathbf{q}_d, \mathbf{f}_d) = \sum_{k=0}^{N} C_d(\mathbf{q}_k, \mathbf{q}_{k+1}, \mathbf{f}_k, \mathbf{f}_{k+1}).$$

We want to find $\mathbf{q}_d$ that minimizes J_d. We chose to minimize control force, $\mathbf{f}_d$, although we could have easily chosen to minimize time or some other parameter depending on the problem at hand. As a simplified example, let us consider the case when

$$C_d(\mathbf{q}_k, \mathbf{q}_{k+1}, \mathbf{f}_k, \mathbf{f}_{k+1}) = \mathbf{f}_k^2.$$

We use the l_2-norm as the measure of control, i.e., we want to minimize

$$\sum_{k=0}^{N} \mathbf{f}_k^2.$$

2.4. **Optimization.** We are faced with an equality constrained nonlinear optimization problem: we seek to find $\mathbf{q}_d$ and $\mathbf{p}_d$ that minimizes J_d subject to the boundary conditions and constraints in (2.3). This optimal control problem can be solved using sequential quadratic programming (SQP), which is implemented as fmincon in Matlab.

3. Results

Since a demonstration balloon flight is planned for the Mojave Desert, we used wind field data computed using the WRF model (see Appendix 5.1) from the same region starting on July 5, 2005 at 12:00pm GMT. Specifically, we targeted a region nearby $(-116°E, 36°N)$ at an altitude of 3500m. Thus, the wind field is a function of two spatial dimensions and time.

The initial and final positions were chosen to be about 100km apart fitting the specifications of the medium-scale problem. We required that the initial and final velocity were zero.

We made a movie with 205 frames that shows the progression of the balloon along its trajectory in the time-dependent wind field. Figures (3.1) - (3.5) are five frames of this movie and show the optimal path at different points in time.

These results suggest that DMOC is able to find a near-optimal path which is satisfactory for the medium-scale problem. Because SQP is a local optimization routine, the optimal trajectory depends heavily on the initial guess. Fortunately, we are not interested in the global minimum although choosing a better initial guess would result in a better local minimum. In our case, we used a linear initial guess. We could substantially improve the results if we were to choose an initial guess that accounts for the wind field.

We also were able to increase the number of discretization points by using the result from one run of DMOC as the initial guess for a subsequent run with more descretization points. In this case, we started with $N = 50$ and used the result as an initial guess for $N = 101$. We did this again to get the optimal path for $N = 203$. This allows us to get results for a large N fairly inexpensively since the most time consuming step is the first run.
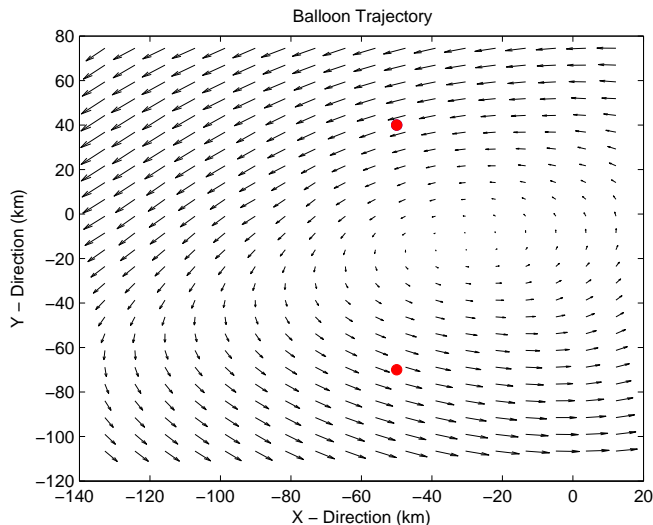

FIGURE 3.1. The balloon's initial position is the upper red dot and its target is the lower red dot. We display the wind field at hour 0, which corresponds to July 5, 2005 at 12:00pm GMT.
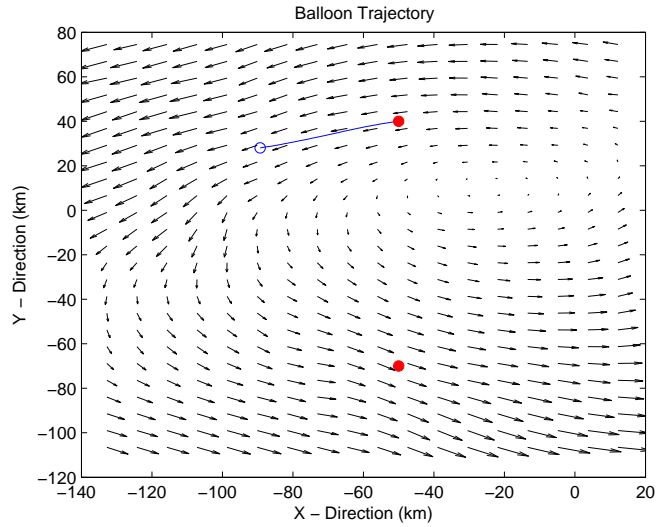
FIGURE 3.2. The balloon's trajectory after 2.84 hours. As expected, the balloon's path seems to closely follow the direction of the wind.
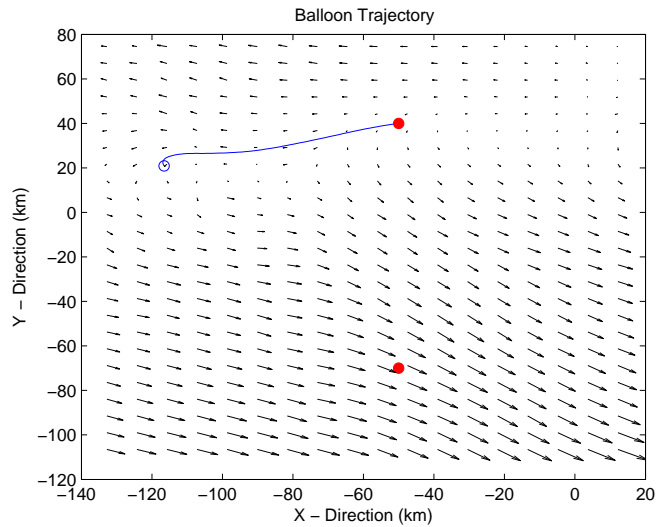

FIGURE 3.3. The balloon's trajectory after 5.96 hours. Interestingly, the balloon has found a region where it is able to turn toward its destination. In this region, the wind is relatively calm although it pushes the balloon in the right direction. The calm wind allows the balloon to easily make maneuvers (i.e., minimal control) to change its flight path.
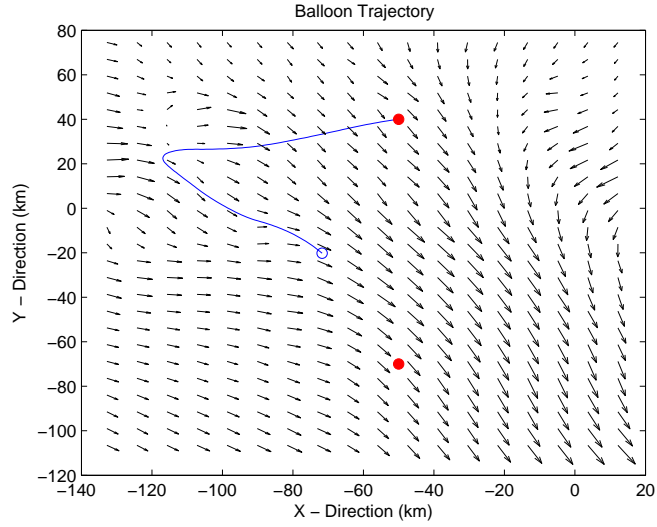
FIGURE 3.4. The balloon's trajectory after 10.86 hours. It appears that the wind is able to carry the balloon toward its final destination. The only important piece left is to ensure that the balloon is able to stop at the target to satisfy the velocity boundary condition.
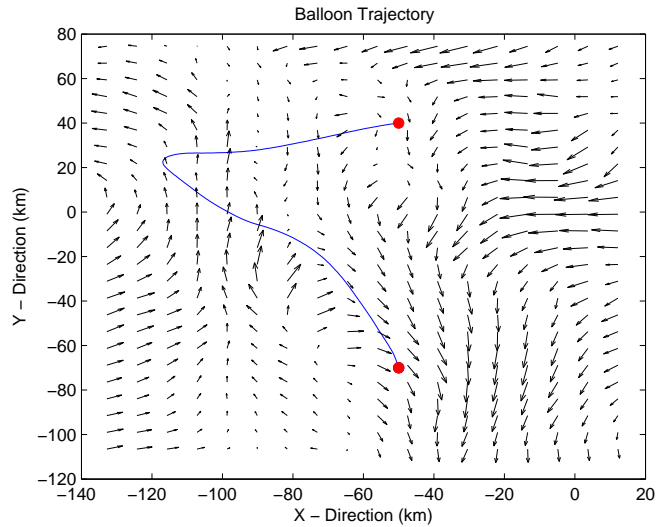

FIGURE 3.5. The balloon's optimal path requires 14.48 hours. Since the wind at that location is significant, it requires a strong force for the balloon to reach zero velocity.

4. Future Research Goals

4.1. Three-Dimensions. We are currently working to expand the model to three dimensions, however doing so requires a slight change in the method of obtaining the wind field - see Appendix (5.1). The current method provides us with non-uniform data (particularly in the z-direction), interpolation of which significantly slows the optimization (by more than 100 times). We are currently exploring methods that use faster interpolation in the z-direction that may sample directly from the output of WRF instead of requiring pre-processing.

Incorporating time into the three dimensional problem posses further difficulties since a four-dimensional interpolation may significantly slow the optimization. However, a receding-horizon approach [8] may be used as an alternative.

4.2. Real-Time Optimization. Probabilistic road-map methods have been shown to be useful for real-time path planning. The method is divided into a learning phase and a query phase [10]. In the learning phase, we randomly sample the configuration space of the balloon and then use some fast local trajectory routine to connect these so-called free configurations. One can think of this roadmap as a graph whose nodes are the free configurations and whose edges are the paths generated by the local path planner. In the query phase, the start and goal configurations are connected to the graph.
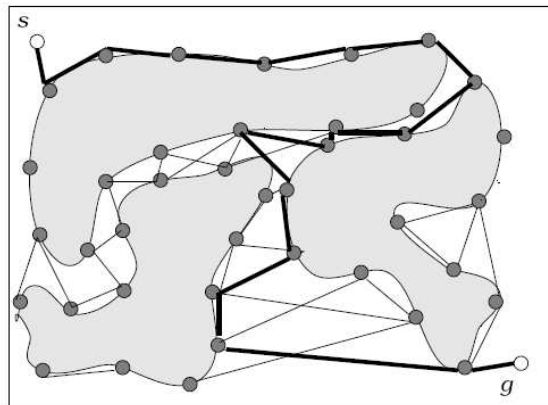

FIGURE 4.1. Example of an obstacle-based probabilistic roadmap. *s* and *g* are the start and goal configurations. A path is found by searching over the roadmap. Image was taken from [14].

One possible local trajectories planner is based on motion primitives [7, 1], which are essentially precomputed (i.e., off-line) trajectories and stored in a library for fast retrieval. These trajectories can be computed using DMOC (and, thus, locally optimal) or recorded maneuvers from a field test. However, with wind forces, such an approach may not be feasible. We are considering possible alternatives, such as sampling the control force space instead of the state space of the system. Alternatively, a machine-learning based approach may work as well.

5. Appendix

5.1. **The Weather Research and Forecasting Model.** The influence of wind is a significant component of the constraint equations. Since we are investigating the problem of a balloon appropriately exploiting winds to reach high priority targets, it is important to obtain actual wind fields for the region of interest. To do so, we use the Weather Research and Forecasting (WRF) model. It is a numerical, mesoscale weather prediction system used for both research and forecasting applications [6]. For our purposes, it is capable of providing wind velocities (i.e. speed and direction) at different latitudes and longitudes. As an example, we considered a region of the Mojave Desert on July 5, 2005 at 12:00pm GMT. We chose the Mojave Desert because it is the likely location of a balloon demonstration flight currently planned to take place in 2009.

5.1.1. *Vertical Coordinate.* WRF uses a "terrain-following hydrostatic-pressure" [6] vertical coordinate, more commonly known as the σ coordinate, for its computation. Sigma is used as the vertical coordinate as opposed to altitude because it is preferred for ease of calculation in global climate models. It is the ratio of the pressure at a point in the atmosphere to the pressure of the surface of the Earth beneath it

$$\eta = \frac{p_h - p_{ht}}{p_{hs} - p_{ht}}$$

where p_h is the hydrostatic component of the pressure, and p_{hs} and p_{ht} are the hydrostatic component of the pressure at the surface and top boundary respectively. It clearly follows that at the surface, $\eta = 1$ and at the top boundary, $\eta = 0$.
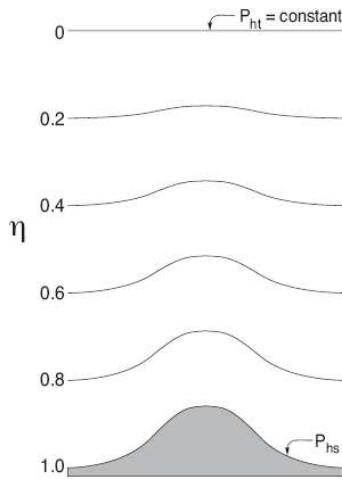

FIGURE 5.1. Example of sigma coordinate at different values of η for an uneven terrain. It is clear that the altitude is not constant for a given η. Image was taken from [6].

5.1.2. *Interpolating onto a Cartesian Grid.* Unfortunately, WRF gives the wind speeds on a curvilinear grid
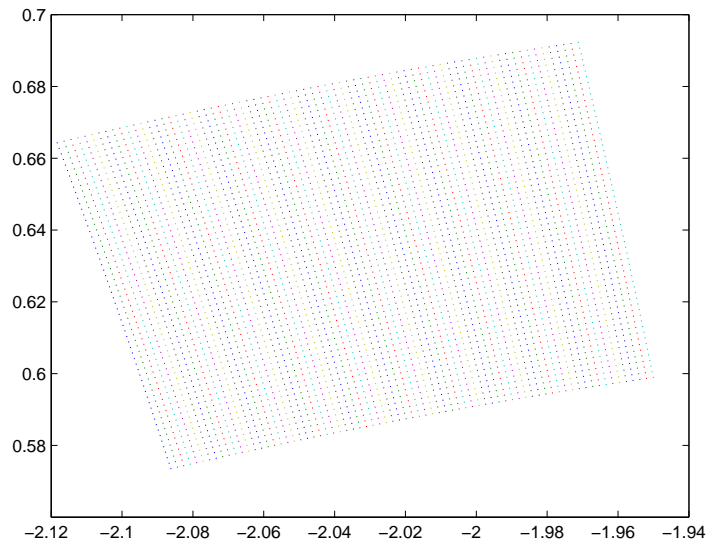
FIGURE 5.2. Curvilinear grid used by WRF

yet we would like it to have the wind speeds on a uniform, rectangular Cartesian grid. As mentioned, interpolation of uniform data is significantly faster and improves the speed of optimization.
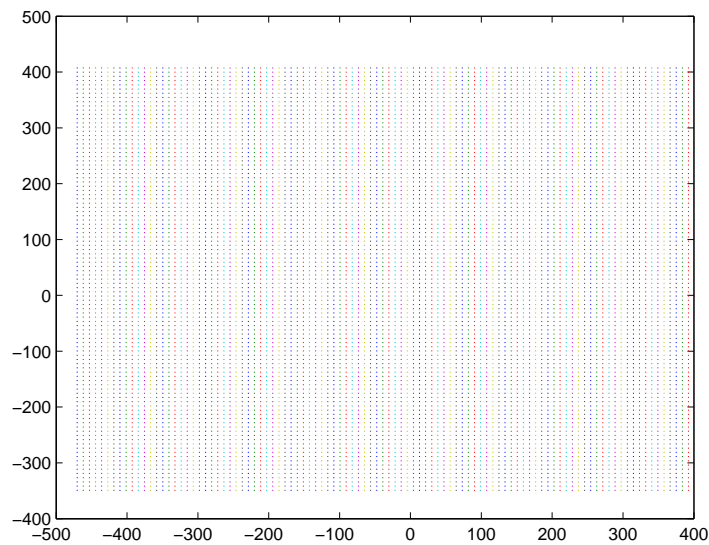

FIGURE 5.3. Uniform, rectangular Cartesian grid onto which we interpolate the WRF output

To do this, we must first interpolate all the necessary data (which we will show are the wind speeds and the geopotential height) onto the grid. We must also take into the account that the data is staggered on an Arakawa-C grid.

Additionally, we make a change of coordinates from latitude and longitude to Cartesian distance

$$(5.1) \qquad x = \frac{\pi}{180°} \cdot r \cdot \cos(\phi) \cdot (\lambda - \lambda_0),$$

$$(5.2) \qquad y = \frac{\pi}{180°} \cdot r \cdot (\phi - \phi_0),$$

where ϕ is latitude, λ is longitude, and $r = 6,378 \cdot 10^3 m$ is the radius of the Earth (for simplicity, we are assuming that the Earth is spherical). We note that (λ_0, ϕ_0) is the origin, which in the case of Mojave Desert, will be $(-116°E, 36°N)$.

The WRF model provides us with a table of discrete altitudes (obtained by dividing the geopotential height by Earth's gravity) and wind velocities as functions of position and the sigma level, i.e.,

$$z = z(x, y, \sigma)$$
$$\mathbf{v} = \mathbf{v}(x, y, \sigma).$$

For our purposes, we need wind velocities as functions of x,y,z and thus we retabulate the wind velocities so that they are functions of projected position on the ground and altitude, i.e.,

$$\tilde{\mathbf{v}} = \tilde{\mathbf{v}}(x, y, z).$$

We do this via interpolation so that for a fixed x, y, $\tilde{\mathbf{v}}$ is

$$\tilde{\mathbf{v}}(x, y, z(\sigma)) = \mathbf{v}(x, y, \sigma).$$

Current implementation of such interpolation is quite crude. We are considering alternative approaches that improve the computation speed and the accuracy of the resulting wind data. This is a component of the future research goals - see Section (4.1).

References

[1] C. Dever, B. Mettler, E. Feron, and J. Popovic. Nonlinear Trajectory Generation for Autonomous Vehicles via Parameterized Maneuver Classes. *Journal of Guidance, Control, and Dynamics*, 29(2):289–302, March-April 2006.

[2] A. Elfes et al. Autonomous flight control for a Titan exploration aerobot. In *International Symposium on Artificial Intelligence, Robotics and Automation in Space*, Munich, Germany, 2005.

[3] E. R. Stofan et al. The lakes of Titan. *Nature*, 445:61–64, 2007.

[4] J. C. Zarnecki et al. A soft solid surface on Titan as revealed by the Huygens Surface Science Package. *Nature*, 438:792–295, 2005.

[5] R. D. Lorenz et al. The Sand Seas of Titan: Cassini RADAR Observations of Longitudinal Dunes. *Science*, 312:724–727, 2006.

[6] W. Skamarock et al. A Description of the Advanced Research WRF Version 2. Ncar Technical Note, National Center for Atmospheric Research, Boulder, Colorado, USA, 2007.

[7] E. Frazzoli, M. A. Dahleh, and E. Feron. Maneuver-Based Motion Planning for Nonlinear Systems With Symmetries. *IEEE Transations on Robotics and Automation*, 21(6):1077–1091, December 2005.

[8] T. Inanc, S. C. Shadden, and J. E. Marsden. Optimal Trajectory Generation in Ocean Flows. In *Proceedings of the 24th American Control Conference*, Portland, Oregon, USA, 2005.

[9] O. Junge, J. E. Marsden, and S. Ober-Blobaum. Discrete Mechanics and Optimal Control. In *Proceedings of the 16th IFAC World Congress*, 2005.

[10] L. E. Kavraki, P. Svestka, J. Latombe, and M. H. Overmars. Probabilistic Roadmaps for Path Planning in High-Dimensional Configuration Spaces. *IEEE Transactions on Robotics and Automation*, 12(4):566–580, August 1996.

[11] M. Kobilarov, M. Desbrun, J. E. Marsden, and G. S. Sukhatme. A Discrete Geometric Optimal Control Framework for Systems with Symmetries. In *Robotics: Science and Systems*, 2007.

[12] R. D. Lorenze. Post-Cassini Exploration of Titan: Science Rationale and Mission Concepts. *Journal of the British Interplanetary Society*, 53:218–234, 2000.

[13] K. Reh, D. Matson, and J. Lunine. TSSM Architecture and Orbiter Design. Unpublished presentation, July 9 2008.

[14] Y. Wu. An Obstacle Based Probabilistic Roadmap Method for Path Planning. Master's thesis, Texas A&M University, August 1996.